

The little galaxy that could: Kinematics of Camelopardalis B

Ayesha Begum¹

NCRA/TIFR, P. O. Bag 3, Ganeshkhind, Pune 411007, India.

Jayaram N. Chengalur²

NCRA/TIFR, P. O. Bag 3, Ganeshkhind, Pune 411007, India.

Ulrich Hopp³

Universitätssternwarte Munchen, Scheinerstrasse 1, D-81679 Munchen, Germany.

Abstract

We present deep, high velocity resolution ($\sim 1.6 \text{ km sec}^{-1}$) Giant Meterwave Radio Telescope HI 21cm synthesis images, as well as optical broad band images, for the faint ($M_B \sim -10.9$) dwarf irregular galaxy Camelopardalis B.

We find that the HI in the galaxy has a regular velocity field, consistent with rotational motion. Further, the implied kinematical major axis is well aligned with the major axis of both the HI flux distribution as well as that of the optical emission. Camelopardalis B is the faintest known galaxy with such relatively well behaved kinematics.

From the HI velocity field we derive a rotation curve for the galaxy using the usual tilted ring model. The rotation curve can be measured out to galacto-centric distances > 4 times the optical scale length. The peak (inclination corrected) rotation velocity v_o is only $\sim 7 \text{ km sec}^{-1}$ – the high velocity resolution of our observations were hence critical to measuring the rotation curve. Further, the peak rotational velocity is comparable to the random velocity σ of the gas, i.e. $v_o/\sigma \sim 1$. This makes it crucial to correct the observed rotation velocities for random motions before trying to use the kinematics to construct mass models for the galaxy. After applying this correction we find a corrected peak rotation velocity of $\sim 20 \text{ km sec}^{-1}$.

On fitting mass models to the corrected rotation curve we find that the kinematics of Camelopardalis B can be well fit with a modified isothermal halo with central density $\rho_0 \sim 12 M_\odot \text{ pc}^{-3}$. This central density is well determined, i.e. it has a very weak dependence on the assumed mass to light ratio of the stellar disk. We also find that the corrected rotation curve cannot be fit with an NFW halo regardless of the assumed mass to light ratio.

Finally we compile from the literature a sample of galaxies (ranging from normal spirals to faint dwarfs) with rotation curves obtained from HI synthesis observations. The complete sample covers a luminosity range of ~ 12 magnitudes. From this sample we find (i) that Camelopardalis B lies on the Tully-Fisher relation defined by these galaxies, provided we use the pressure support corrected rotation velocity, and (ii) a weak trend for increasing halo central density with decreasing galaxy size. Such a trend is expected in hierarchical models of halo formation.

Key words: dark matter, Galaxy: kinematics and dynamics, galaxies: individual: Camelopardalis B, galaxies: dwarf, line: profiles
PACS: 95.75.Kk, 95.35.+d, 98.62.Dm, 98.56.Wm

1 Introduction

There are a number of reasons why kinematical studies of faint dwarf galaxies are particularly interesting. The first is related to the structure of the dark matter halos of galaxies. Traditionally, dark matter halos have been modeled as “modified isothermal” halos for which the density is constant in the central regions. However, numerical simulations of galaxy formation in hierarchical structure formation models (such as the standard CDM or Λ CDM models) predict that galaxy halos should have cuspy central density distributions (Navarro, Frenk & White 1996, Klypin et al. 2001). In particular, for the popular Navarro, Frenk & White (1996) model, (generally referred to as the “NFW” halo), the density in the central regions increases as r^{-1} . Unfortunately, it turns out that it is difficult to distinguish between isothermal and NFW halos from the observed kinematics of normal spiral galaxies. This is because the gravitational force in the central parts of these galaxies is usually dominated by the mass of the stellar disk. Disentangling the contribution from the dark matter halo hence requires knowledge of the mass to light ratio (M/L) of the stellar disk, which is often poorly constrained. Depending on the assumed disk M/L ratio, equally good fits to the observed kinematics can be obtained using either isothermal halos or NFW halos (see eg. Navarro 1998). Dwarf galaxies, on the other hand, are often dark matter dominated, even in their inner parts, (eg. DDO154, Carignan & Freeman 1988) and consequently their kinematics can be used to constrain the structure of their dark matter halos with minimum uncertainties due to the unknown M/L ratio of the stellar disk.

¹ ayesha@ncra.tifr.res.in

² chengalu@ncra.tifr.res.in

³ hopp@usm.uni-muenchen.de

Apart from the shapes of galaxy halos, numerical simulations also predict correlations between various physical parameters of the halo, most notably between the characteristic density and the virial mass (eg. Navarro, Frenk & White 1997). The characteristic density is found to anti-correlate with the virial mass, i.e. the lowest mass halos have the highest densities. In hierarchical scenarios the low mass halos form at the earliest times (at which time the background density is the highest) and if there is a constant relation between the background density and the characteristic density of the collapsed halo then such a relation is to be expected. The correlation found in numerical simulations is however both weak (a large change in the virial mass of the halo leads to relatively small changes in the characteristic density) and noisy. To test whether such correlations are present in real galaxies it is useful to have data on as wide a range of galaxy masses as possible. While there is already a wealth of kinematical data for bright spiral galaxies, the number of dwarf galaxies, in particular extremely faint (fainter than $M_B \sim -12$) dwarf galaxies, for which good kinematical data is available, is very limited.

Finally, even from a purely phenomenological point of view, the kinematics of extremely faint dwarf irregular galaxies has been the subject of interest from some time now. This is because it is unclear whether the faintest dwarf irregular galaxies are rotationally supported or not. In a systematic study of 9 faint dwarf galaxies Lo, Sargent & Young (1993) found that only two galaxies showed ordered velocity fields, the remaining galaxies all had chaotic velocity fields. Further, independent observations of the extremely faint dwarf galaxy GR8, ($M_B \sim -11.0$, Carignan, Beaulieu & Freeman 1990) showed that although the galaxy had a somewhat ordered HI velocity field, the implied kinematical major axis was perpendicular to the major axis of the optical and HI disk. Similarly, Côté, Carignan & Freeman (2000) found an ordered velocity field for SDIG ($M_B \approx -11.3$), but again the kinematical major axis was found to be perpendicular to the major axis of the optical disk. All of this lead Côté, Carignan & Freeman (2000) to suggest that normal rotation is seen only in dwarfs brighter than $M_B \sim -14$, and that by $M_B \sim -13$ one begins to find systems with misaligned axis, and other kinematical peculiarities. These peculiarities make it difficult, if not impossible to model the kinematics of these galaxies using traditional mass models. This is unfortunate, since it is these very faint systems (which presumably formed at the earliest epochs and are the most dark matter dominated) which could be particularly useful in determining dark halo properties.

We present here deep, high velocity resolution, Giant Meterwave Radio Telescope (GMRT) observations of the faint ($M_B \sim -10.9$) dwarf irregular galaxy Camelopardalis B. We find that the galaxy has a very well ordered velocity field, with no sign of major kinematical peculiarities, despite the fact that the peak (inclination corrected) rotation velocity is only ~ 7 km/s. The rest of this paper is divided as follows. Details of the observational setup and procedure

(both optical and HI 21cm) can be found in section 2. The kinematics of the HI disk and derivation of the rotation curve are presented in section 4, mass models for Cam B are presented in section 5. Finally in section 6 we discuss the kinematics of Cam B in light of the various issues discussed above. Throughout this paper we use a distance of 2.2 Mpc (given by Huchtmeier et al. 2000) for Cam B. Recent HST observations (D. J. Bomans, private communication) confirm this distance estimate.

2 Observations

2.1 Optical Observations

CCD images of Cam B were obtained in Oct. 1996 in the Johnson B and V filters using the focal reducer system CAFOS at the Calar Alto 2.2m telescope. The instrument was equipped with a Tektronix 1024 by 1024 pixel chip with one pixel corresponding to $0.53''$. The usual CCD calibration frames (bias, flats and blank fields) were obtained and standard fields from the list of Landolt (1983) and Christian et al. (1985) were observed in order to determine the absolute photometry. The exposure time on the target galaxy was 1200 and 700 seconds in B and V, respectively and the FWHM seeing of the co-added images was 2.9 arc sec. The total exposure time was divided into three chunks and the pointing centers of the individual exposures were shifted by several tens of arc seconds.

2.2 HI observations

The GMRT observations were conducted during the commissioning phase of the telescope. The setup for the observations is given in Table 1. Absolute flux calibration was done using scans on the standard calibrators 3C48 and 3C286 one of which was observed at the start and end of each observing run. Phase calibration was done using 0410+769 which was observed once every 30 minutes. Cam B has $V_{\text{lsr}} \sim 80 \text{ km sec}^{-1}$, and a velocity width of $\sim 20 \text{ km sec}^{-1}$, inspection of the Dwingeloo survey data toward Cam B shows that no Galactic emission is detected in this velocity range. Bandpass calibration was hence done in the standard way using 3C286 (which itself has no absorption features in the relevant velocity range).

The data were reduced using standard tasks in classic AIPS. For each run, bad visibility points were edited out, after which the data were calibrated. Calibrated data for all runs was combined using DBCON. The GMRT does

Table 1
Parameters of the GMRT observations

Parameters	Value
RA(1950)	$04^h 48^m 03.3^s$
Declination(1950)	$+67^\circ 01' 02''$
Central velocity (heliocentric)	77.0 km sec^{-1}
Date of observations	4–6 Nov 2001
Time on source	16 hrs
Total bandwidth	1.0 MHz
Number of channels	128
Channel separation	1.65 km sec^{-1}
FWHM of synthesized beam	$40'' \times 38''$, $24'' \times 22''$, $16'' \times 14''$
RMS noise per channel	2.5 mJy, 2.0 mJy, 1.6 mJy

not do online doppler tracking – any required doppler shifts have to be applied during the offline analysis. However since the differential doppler shift over our observing interval is much less than the channel width, no correction needed to be applied offline.

3 Results of the Observations

3.1 Optical

Debiasing, flat-fielding and cosmic ray filtering of the CCD images were done in the usual manner, using standard MIDAS routines. After this the individual frames were added after shifting them to a common coordinate system.

Cam B has a relatively irregular optical morphology (see Fig. 3). Because of the bad seeing, it was not possible to determine whether the knotty structures seen in the B band image were barely resolved stars or HII regions, consequently the distance to Cam B could not be estimated from this data set. The irregular morphology however means that the images needed to be smoothed before attempting surface photometry; a gaussian 10 arc sec (FWHM) filter was used for this purpose. Surface photometry was done using the ellipse fitting algorithm of Bender & Möllenhoff (1987). The average ellipticity of Cam B was found to be 0.53 ± 0.16 (corresponding to an inclination of $\sim 65^\circ$ for an intrinsic thickness ratio $q_0 = 0.25$, see section 5). The overall orientation of the optical major axis in the B (V) band data is 210° (199°) degrees, in good agreement

with the orientation of the HI data (see below). At the northern rim, a very faint, fuzzy extension is visible in the V-band (and to a much smaller extent in the B-band) which changes the PA of the outermost isophotes towards a slightly lower value of 189° , but still in good agreement with the overall distribution of the radio data. This extension is related to the color gradient seen in Fig. 1, which shows the surface brightness profiles in the B and V bands. Exponential fits to the surface brightness profiles are shown superposed. The exponential scale lengths are $26.2''$ for the V band and $22.6''$ for the B band. The corresponding linear quantities (at an adopted distance of 2.2 Mpc) are 0.28 kpc and 0.24 kpc respectively. From the figure it can also be seen that $B - V$ is approximately constant in the inner regions of the galaxy (up to $\sim 35''$), while a color gradient is seen in the outer regions of the galaxy. Finally a mask at the 26.5 mag per square arc second level was constructed in order to determine the flux in both filters within the Holmberg isophote. The total B and V magnitudes within the 26.5 mag per square arc sec are found to be 16.71 and 15.91 respectively. The absolute Holmberg magnitude obtained (after correcting for Galactic extinction using $A_B=0.93$ mag and $A_V=0.72$ mag, Schlegel, Finkbeiner & Davis 1998), are $M_B = -10.94$ and $M_V = -11.52$. Note that no correction for internal extinction has been applied. The corresponding B and V luminosities are $L_B = 3.7 \times 10^6 L_\odot$ and $L_V = 3.5 \times 10^6 L_\odot$. We also note that the low value of the central surface brightness (Fig. 1) makes Cam B an LSB galaxy.

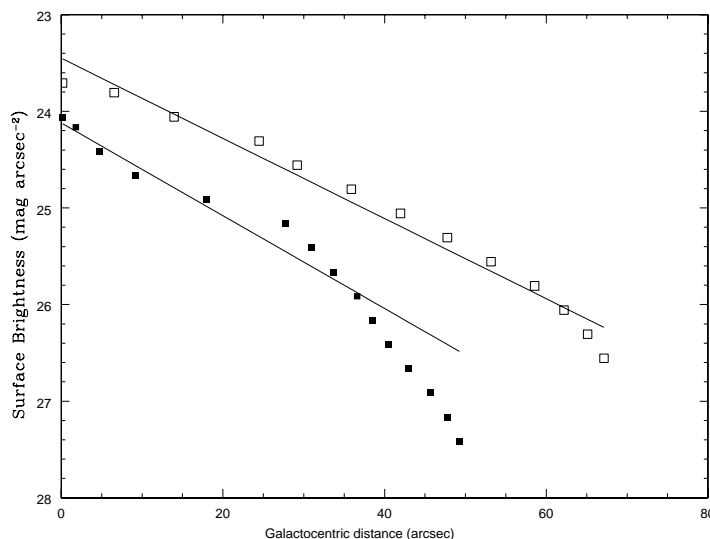


Fig. 1. Surface brightness profile of Cam B in the B (filled squares) and V (empty squares) bands. The best fit exponential profiles are shown superimposed.

3.2 HI Flux and Surface Density Distribution

The GMRT has a hybrid configuration (see Swarup et al. 1991) with 14 of its 30 antennas located in a central compact array with size ≈ 1 km (≈ 5 k λ at 21cm) and the remaining antennas distributed in a roughly “Y” shaped configuration, giving a maximum baseline length of ≈ 25 km (≈ 120 k λ at 21 cm). The baselines obtained from antennas in the central square are similar in length to those of the “D” array of the VLA while the baselines between the arm antennas are comparable in length to the “B” array of the VLA. A single observation with the GMRT hence yields information on both large and small angular scales. Data cubes were therefore made at various (u,v) ranges, viz. 0–5 k λ , 0–10 k λ and 0–15 k λ corresponding to angular resolutions of $40'' \times 38''$, $24'' \times 22''$ and $16'' \times 14''$ respectively. All the data cubes were deconvolved using the the AIPS task IMAGR.

The HI emission from Cam B spanned 18 channels of the spectral cube. A continuum image was made using the average of all the line free channels, no continuum was detected from the disk of Cam B to a 3σ flux limit of 1.8 mJy per beam (for a beam size of $46'' \times 37''$). We also checked for the presence of a few faint small continuum sources in the disk of Cam B by making a high resolution ($3.6'' \times 3.2''$) map – no sources were detected down to a 3σ limit of 0.6 mJy.

The global HI emission profile of Cam B is given in Fig 2. A Gaussian fit to the profile gives a central velocity (heliocentric) of 77.5 ± 1.0 km sec $^{-1}$. The integrated flux is 4.6 ± 0.4 Jy km sec $^{-1}$. These are in excellent agreement with the values of 77.0 ± 1.0 km sec $^{-1}$ and 4.47 Jy km sec $^{-1}$ obtained from single dish observations (Huchtmeier et al. 2000). The excellent agreement between the GMRT flux and the single dish flux shows that the no flux was missed because of the missing short spacings in the interferometric observation. The velocity width at 50 % level of peak emission (ΔV_{50}) is found to be 21.4 ± 1.0 km sec $^{-1}$, which again is in reasonable agreement with the ΔV_{50} value of 18 km sec $^{-1}$ determined from the single dish observations. The HI mass obtained from integrated profile (taking the distance to the galaxy to be 2.2 Mpc) is $5.3 \pm 0.5 \times 10^6 M_{\odot}$, and the M_{HI}/L_B ratio is found to be 1.4 in solar units.

We examined the line profiles at various locations in the galaxy and found that they were (within the noise) symmetric and single peaked. Moment maps i.e. maps of the total integrated flux (moment 0), the flux weighted velocity (moment 1) and the flux weighted velocity dispersion (moment 2) were then made from the data cubes using the AIPS task MOMNT. To obtain the moment maps, lines of sight with a low signal to noise ratio were excluded by applying a mask at 3σ level, σ being the rms noise level in a line free channel.

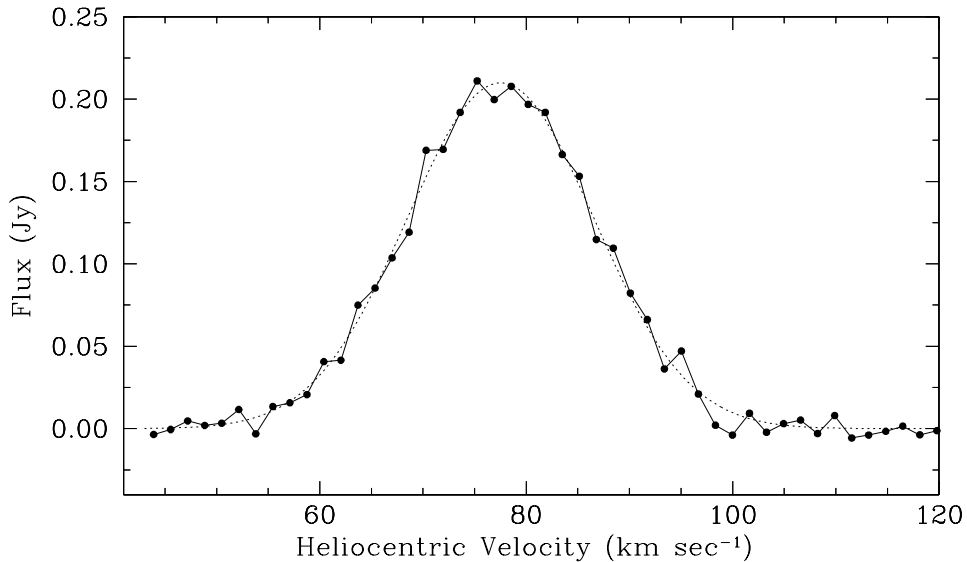


Fig. 2. The global HI profile of Cam B as derived from the GMRT data. The channel separation is 1.65 km sec^{-1} . The dotted line shows a Gaussian fit to the line profile.

Maps of the velocity field and the velocity dispersion were also made in GIPSY using gaussian fitting to the individual profiles. As to be expected, given the simple line profiles, the AIPS moment 1 map and the velocity field obtained using gaussian fits showed excellent agreement. However the AIPS moment 2 map systematically underestimated the velocity dispersion (as obtained from gaussian fitting) particularly near the edges where the signal to noise ratio is low. This can be understood as the effect of the thresholding algorithm used by the MOMNT task to identify the regions with signal. From the gaussian fitting we find that the velocity dispersion σ is $\approx 7.3 \text{ km sec}^{-1}$, and shows no measurable variation across the galaxy. This value of σ and the lack of measurable variation of σ across the galaxy is typical of dwarf galaxies (eg. Lake et al. 1990, Skillman et al. 1988).

Figure 3 shows the integrated HI emission at $40'' \times 38''$ arcsec resolution overlaid on the digitized sky survey image of Cam B. Consistent with the optical image the HI isophotes suggest that galaxy is seen at a fairly high inclination. Figure 4 shows the deprojected radial surface density profile of the HI obtained from fitting elliptical annuli to the HI moment 0 image. A gaussian fit is shown superimposed; as can be seen the surface density $\Sigma_{HI}(r)$ is well represented by a Gaussian:

$$\Sigma_{HI}(r) = \Sigma_0 \times e^{-r^2/2r_0^2} \quad (1)$$

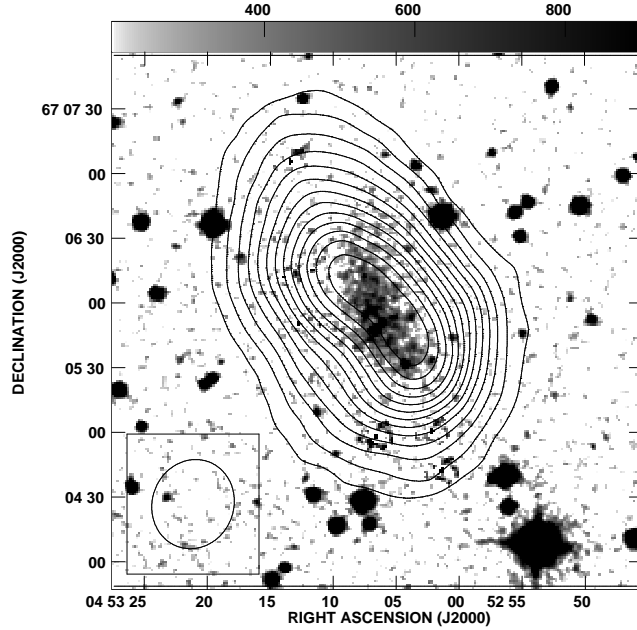


Fig. 3. The digitized Palomar Sky Survey image of Cam B with the GMRT $40'' \times 38''$ resolution integrated HI emission (moment 0) map overlaid. The contour levels are 3.7, 8.8, 19.1, 24.3, 29.4, 34.6, 39.8, 44.9, 50.1, 55.2, 60.4, 65.5 & 70.7 $\times 10^{19}$ atoms cm^{-2} . with $r_0 = 40.7'' \pm 1.6''$ (corresponding to a linear scale of 0.43 kpc) and $\Sigma_0 = 5.9 \pm 0.2 M_\odot \text{pc}^{-2}$.

The inclination of the HI disk was determined from ellipse fitting to the HI isophotes and was found to be 65 ± 5 degrees (where we have assumed an intrinsic thickness ratio $q_0 = 0.25$, see Sec. 5). The position angle obtained from the ellipse fitting was found to be 215 ± 5 degrees. The values of inclination and position angle found from the HI distribution are in good agreement with the values obtained from the optical image (section 3.1).

3.3 HI Kinematics

The velocity field derived from the moment analysis of $24'' \times 22''$ resolution data is shown in Figure 5. The velocity field is regular and the isovelocity contours are approximately parallel, this is the signature of rigid body rotation. The kinematic major axis of the galaxy has position angle $\approx 215^\circ$, i.e. is aligned with the major axis of both the HI distribution (see section 3.2) and the optical image (see section 3.1). Cam B is the faintest galaxy known to show such regular kinematics. It is worth noting that the high velocity resolution (\sim

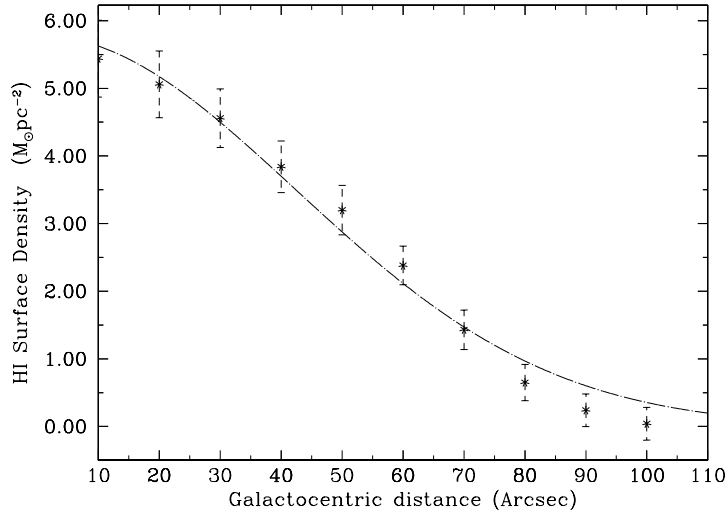


Fig. 4. The HI surface density profile derived from the HI surface density shown in Figure 3. A gaussian fit is shown superimposed.

1.6 km sec¹) of our observations was critical in determining the velocity field. Synthesis observations often use much poorer resolution (eg. Lo, Sargent & Young (1993) used a velocity resolution of ~ 6.2 km sec⁻¹), at these resolutions it would be difficult to discern systematic patterns, if any, in the velocity fields of faint dwarfs.

4 HI Rotation Curve

The rotation curve was derived from the HI velocity field using the usual tilted ring model (Warner et al. 1973). Three different velocity fields were used, viz. those derived from the $40'' \times 38''$, $24'' \times 22''$ and the $16'' \times 14''$ resolution data cubes. An attempt to derive the rotation curve leaving the center and inclination as a free parameters in the fit did not lead to reliable results, consistent with the solid body like rotation field. The centre of the galaxy was hence fixed to be the center of symmetry of the HI moment 0 map and V_{sys} was fixed at the value of 77.0 km sec⁻¹ which was obtained from the single dish profile. Again guided by the optical and HI morphology the inclination of all annuli was fixed at a value of 65° and the position angle at 215° . The rotation curve was then computed using the GIPSY task ROTCUR by breaking up the galaxy into annuli (each of width half that of the synthesized beam) and fitting to the velocity field in each annulus keeping all parameters except the circular velocity V_c fixed.

The derived rotation curve is shown in Fig. 6. The rotation curves obtained from $24'' \times 22''$ and the $16'' \times 14''$ resolution velocity fields agree to within

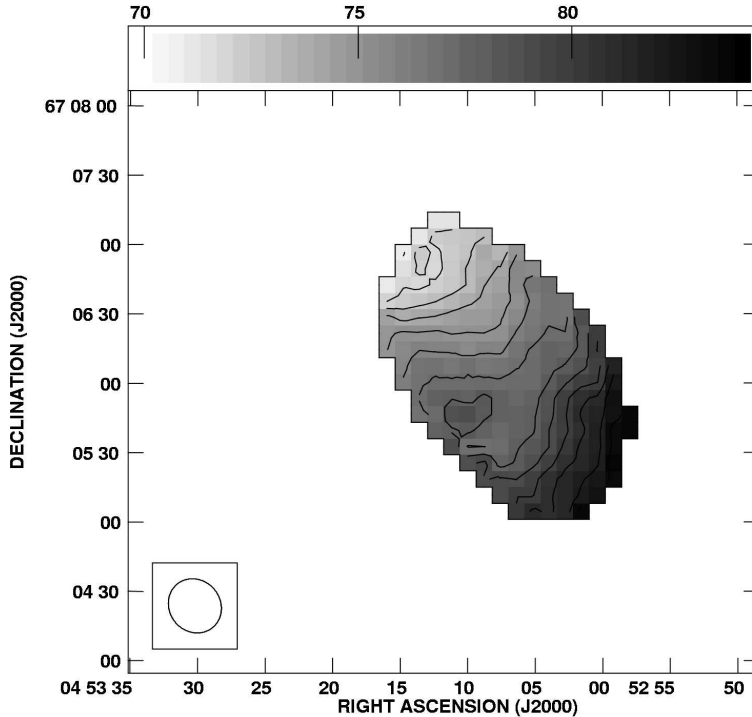


Fig. 5. The HI velocity field of Cam B at $24'' \times 22''$ arcsec resolution. The contours are in steps of 1 km sec^{-1} and range from 70.0 km sec^{-1} (the extreme North West contour) to 84.0 km sec^{-1} (the extreme South East contour).

the error-bars. For the rest of the analysis, the rotation curve obtained from the $24'' \times 22''$ resolution cube is used in the inner region (up to $80''$) of the galaxy while the outermost points (from $80'' - 120''$) are taken from the lower resolution $40'' \times 38''$ resolution velocity field. From Fig. 6 one can see that the maximum velocity reached by the rotation curve ($\approx 7.0 \text{ km sec}^{-1}$) is comparable to the observed velocity dispersion i.e $V_{max}/\sigma \approx 1.0$.

The effect of beam smearing in the derivation of HI rotation curves has been the subject of recent debate. To estimate the effect of beam smearing on our data we created a model data cube using the observed rotation curve and column density profile and smoothed it to a beam size of $24'' \times 22''$ using the task GALMOD in GIPSY. Moment maps were then made of this data cube and a rotation curve was derived in exactly the same manner as for the real data. This model rotation curve is shown in Fig. 7 as a dotted line. As can be seen, this agrees very well with the observed rotation curve. This suggests that beam smearing has only a small effect for this data set.

Since for Cam B the maximum rotation velocity obtained is comparable to the velocity dispersion, random motions provide significant dynamical support to the disk. Equivalently, the observed circular velocity significantly underestimates the centripetal force and hence the implied dynamical mass. The observed rotation velocities hence need to be corrected before trying to estimate

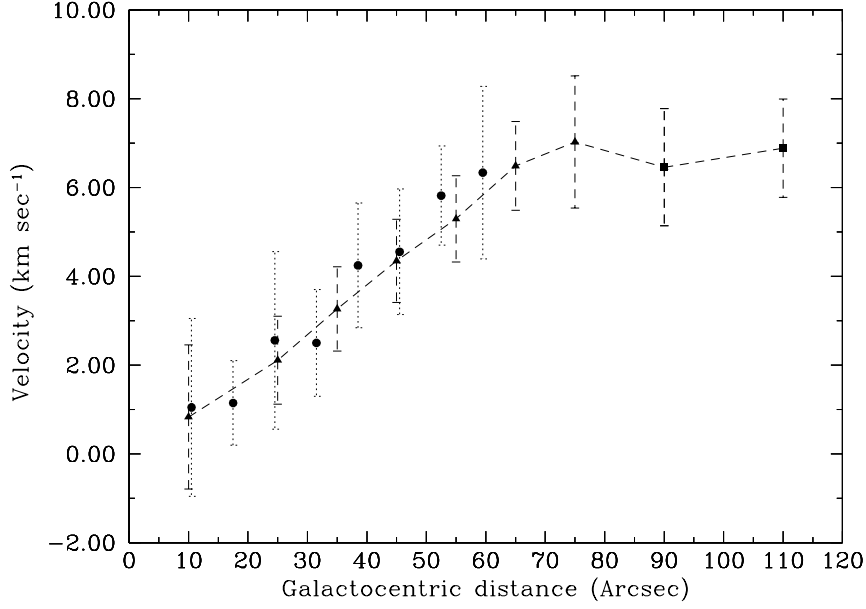


Fig. 6. Rotation curve derived from the intensity weighted velocity field. Filled circles, triangles and squares show the rotation curve derived from the $16'' \times 14''$, $24'' \times 22''$ and $40'' \times 38''$ resolution velocity fields respectively. The dotted line shows the adopted rotation curve.

the dynamical mass. This correction, generally termed an “asymmetric drift” correction is given by (eg. Muere et al. 1996; note that the formula below is slightly different from the one in Muere et al. 1996 since we have used a sech^2 profile in the vertical direction instead of an exponential one)

$$v_c^2 = v_o^2 - r \times \sigma^2 \left[\frac{d}{dr}(\ln \Sigma_{HI}) + \frac{d}{dr}(\ln \sigma^2) - \frac{d}{dr}(\ln 2h_z) \right],$$

where v_c is the true circular velocity, v_o is the observed rotation velocity, σ is the velocity dispersion, and h_z is the scale height of the disk. Strictly speaking, asymmetric drift corrections are applicable to collisionless stellar systems for which the magnitude of the random motions is much smaller than that of the rotation velocity. However, it is often used even for gaseous disks, where the assumption being made is that the pressure support can be approximated as the gas density times the square of the random velocity. For the case of Cam B, in the absence of any direct measurement of h_z we assume $d(\ln(h_z))/dr = 0$, (i.e. that the scale height does not change with radius) and also use the fact that σ^2 is constant across the galaxy, to get:

$$v_c^2 = v_o^2 - r \times \sigma^2 \left[\frac{d}{dr}(\ln \Sigma_{HI}) \right]. \quad (2)$$

Using the fitted Gaussian profile to the radial surface density distribution, (see

eqn 1) we obtain

$$v_c^2 = v_o^2 + r^2\sigma^2/r_0^2. \quad (3)$$

Finally, the observed σ_{obs} of $7.3 \text{ km}^2 \text{ sec}^{-2}$ (see section 3.2) needs to be corrected for the finite velocity resolution of the observations as well as the contribution of the rotation velocity gradient over the finite size of the beam. The correction is:

$$\sigma_{true}^2 = \sigma_{obs}^2 - \Delta v^2 - \frac{1}{2}b^2(\nabla v_o)^2,$$

where σ_{true} is the true velocity dispersion, Δv is the channel width, b characterizes the beam width (i.e. the beam is assumed to be of form e^{-x^2/b^2}) and v_o is the observed rotation velocity. This correction turns out to be small; after putting in the appropriate values in the above equation we get $\sigma_{true}^2 \approx 49.0 \text{ km}^2 \text{ sec}^{-2}$. Substituting this value back into Eqn. (3) to get the final ‘‘asymmetric drift’’ corrected rotation curve, which is shown as the dash dot line in Fig. 7.

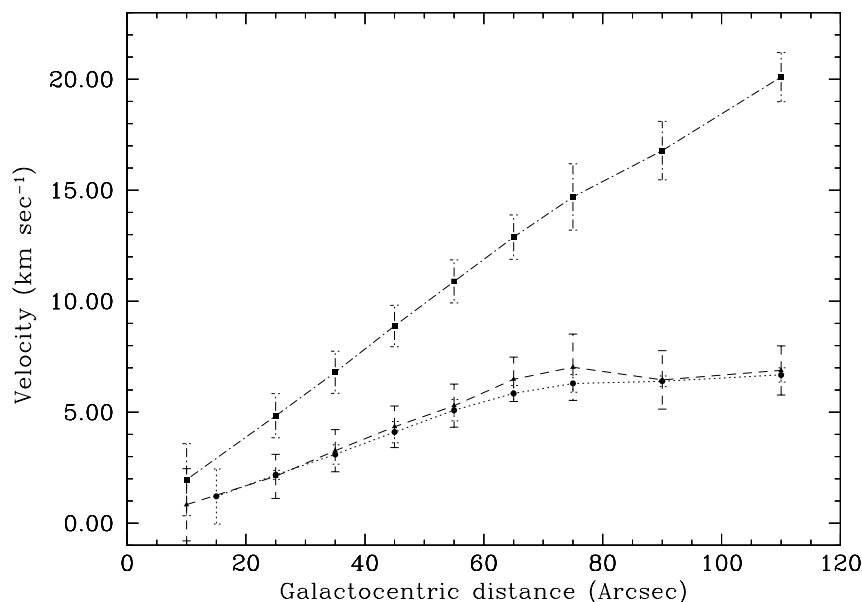


Fig. 7. The final adopted rotation curve (dashes), the rotation curve after beam smearing (dots) and the rotation curve after applying the asymmetric drift correction (dash dots).

5 Mass Models

In this section we attempt to decompose the mass distribution of Cam B into contributions from the stellar disk, the gaseous disk and the dark matter (DM) halo.

For the stellar disk we assume a constant (M/L_V) ratio Υ_V with the radius. Recall from section 3.1 that the galaxy color was approximately constant in the inner regions (within $\sim 35''$), but there is a gradient in the color in the outer parts. This suggests that there could be a gradient in mass to light ratio in the outer parts of the galaxy. However, since it turns out that the stellar disk makes a negligible contribution to the total mass in the outer parts of the galaxy, the assumption of a constant Υ_V throughout the galaxy will not lead to substantial uncertainty in the mass of the dark halo. Similarly, the deviations from the exponential fit in the outer parts of the galaxy (which are related to the very faint extensions to the north in Fig. 3) has only a small effect on the fitted mass model. We hence take the stellar disk to be an exponential disk (see section 3.1) with an intrinsic thickness ratio (q_o) of 0.25 (see below). We further assume that the density distribution in the vertical(z), direction falls off like $\text{sech}^2(z/z_0)$ with z_0 independent of galacto-centric radius. This is a reasonable approximation for disk galaxies (see eg. van der Kruit & Searle 1981, de Grijs & Peletier 1997). In the absence of any prior knowledge of Υ_V , it is taken to be a free parameter during the modeling.

The contribution of the gaseous disk to the observed rotation curve is calculated using HI surface mass density profile given in Fig. 4. The contribution of primordial Helium is taken into account by multiplying HI densities by a factor of 1.4. There is little evidence that dwarf galaxies contain substantial amounts of molecular gas (see eg. Israel, Tacconi & Bass 1995, Taylor, Kobulnicky & Skillman 1998), so no correction has been made for molecular gas. We also neglect the contribution of ionized gas, if any. Not much is known about the vertical distribution of gas in disk galaxies, however there is some evidence for similar vertical distributions of the HI and stellar disk (eg. Bottema, Shostak & van der Kruit 1986). For the intrinsic thickness ratio of the gaseous disk we hence assume $q_0 = 0.25$ and also assume that the shape of the profile in the vertical direction is given by $\text{sech}^2(z/z_0)$. To check the validity of these assumptions we tried modeling the HI distribution and velocity field with various vertical profiles and intrinsic thickness ratios using the GIPSY task GALMOD. It was found that the best (visual) match between the model and the observed maps were obtained with a $\text{sech}^2(z/z_0)$ profile and an intrinsic thickness ratio of 0.25. The geometries of all the disk components being thus fixed, the circular velocities of the disk components were computed using the formulae given by Casertano (1983).

For the dark matter we considered two types of density profiles, a modified isothermal halo and an NFW halo. The modified isothermal halo has a density profile given by:

$$\rho_{iso}(r) = \rho_0[1 + (r/r_c)^2]^{-1},$$

where, ρ_0 is the central density of the halo and r_c is the core radius. The corresponding circular velocity is given by

$$v(R) = \sqrt{4\pi G \rho_0 r_c^2 [1 - \frac{r}{r_c} \tan^{-1}(\frac{r}{r_c})]}.$$

The NFW halo density is given by

$$\rho_{NFW}(r) = \rho_i / [(r/r_s)(1 + r/r_s)^2],$$

where, r_s is the characteristic radius of the halo and ρ_i is the characteristic density. The circular velocity can be written as:

$$v(R) = v_{200} \sqrt{\frac{\ln(1+cx) - cx/(1+cx)}{x[\ln(1+c) - c/(1+c)]}},$$

where, $c = r_{200}/r_s$, $x = r/r_{200}$; r_{200} is the distance at which the mean density of the halo is equal to 200 times the critical density and v_{200} is the circular velocity at this radius.

We consider first fits using a modified isothermal halo. Because the rotation curve (Fig. 7) is rising till the last measured point, the parameter r_c cannot be constrained. (To constrain r_c one needs the rotation curve to transition from rising linearly to being more or less flat, as is typically seen for spiral galaxies). We are therefore left with two free parameters, viz., the mass to light ratio of the stellar disk, Υ_V , and the core density of the halo ρ_0 . The modeling procedure consists of a χ^2 minimization of

$$v_c^2 - \Upsilon_V v_*^2 - v_g^2 - v_h^2(\rho_0),$$

where, v_c is the corrected rotation velocity (see eqn. 3), v_* , v_g , and v_h are the circular speeds of the stellar disk, gaseous disk and the dark halo respectively. This minimization was done using the GIPSY task ROTMAS. Since there are heuristics involved in computing the error bars on v_c , it is not possible to rigorously translate the minimum χ^2 value into a confidence interval for the parameters of the fit. However, a lower χ^2 value does imply a better fit (see also the discussion in van den Bosch & Swaters 2001). We found that the χ^2 continuously decreases as Υ_V decreases. The observed (B-V) for Cam B is 0.8, which corresponds to Υ_V is ~ 1.8 (from the low metallicity Bruzual & Charlot SPS model using a modified Salpeter IMF, Bell & de Jong 2001). Using this value of Υ_V gives $\rho_0 = 12.0 \times 10^{-3} M_\odot pc^{-3}$ and a reduced χ^2 of 1.9. For comparison, fixing Υ_V to be 1.0, gives a reduced $\chi^2=0.96$ and a best

fitting $\rho_0 = 12.4 \times 10^{-3} M_{\odot} \text{pc}^{-3}$. At the two extremes, if we assume $\Upsilon_V = 0$ we get $\rho_0 = 14.0 \times 10^{-3} M_{\odot} \text{pc}^{-3}$ (and a reduced $\chi^2=0.2$) and $\Upsilon_V = 2$ (which substantially overpredicts the observed rotation curve at small radii, and is hence an upper limit to Υ_V) we get $\rho_0 = 11.0 \times 10^{-3} M_{\odot} \text{pc}^{-3}$ (and a reduced $\chi^2=2.2$). As can be seen the central halo density ρ_0 is relatively insensitive to the assumed Υ_V , and is well determined. To illustrate the general quality of fit we show in Fig. 8 the mass decomposition for a modified isothermal halo using $\Upsilon_V = 0.2$.

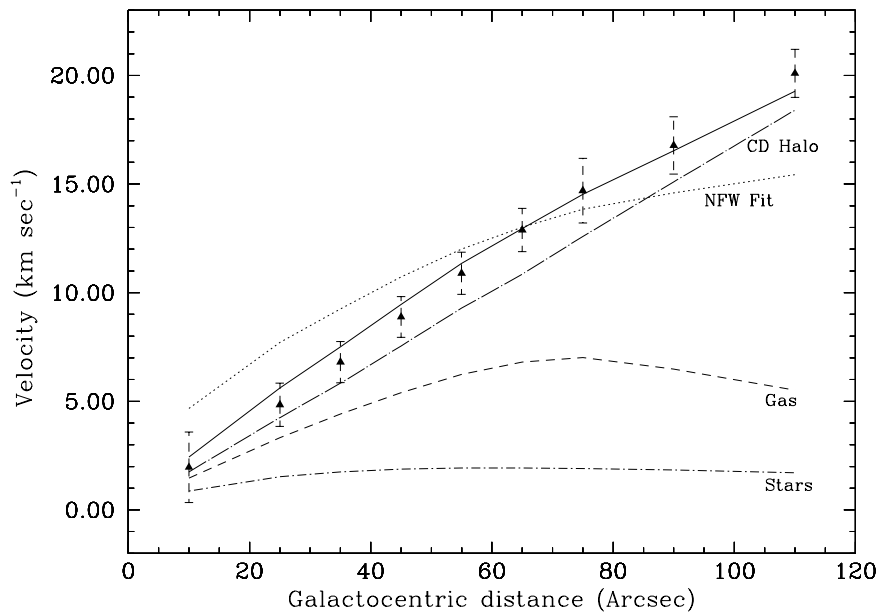


Fig. 8. Mass models for Cam B using the corrected rotation curve. The points are the observed data. The total mass of gaseous disk (dashed line) is $6.6 \times 10^6 M_{\odot}$. The stellar disk (short dash dot line) has $\Upsilon_V = 0.2$, giving a stellar mass of $0.7 \times 10^6 M_{\odot}$. The best fit total rotation curve for the constant density halo model is shown as a solid line, while the contribution of the halo itself is shown as a long dash dot line (the halo density is density $\rho_0 = 13.7 \times 10^{-3} M_{\odot} \text{pc}^{-3}$). The best fit total rotation curve for an NFW type halo (for $c = 1.0$ and $\Upsilon_V = 0.0$) is shown as a dotted line. See the text for more details.

A similar procedure was tried using a dark matter halo of the NFW type, but no reasonable fit could be obtained for any value of Υ_V . Essentially Cam B is dark matter dominated and has a linear rotation curve while the NFW halo provides a poor fit for linear rotation curves. As an illustration we show in Fig. 8 the best fit rotation curve for an NFW halo with $c = 1.0$, $\Upsilon_V = 0.0$, and v_{200} chosen to minimize the χ^2 . These are already unphysical values for these parameters, and increasing either c or Υ_V only worsens the quality of the fit.

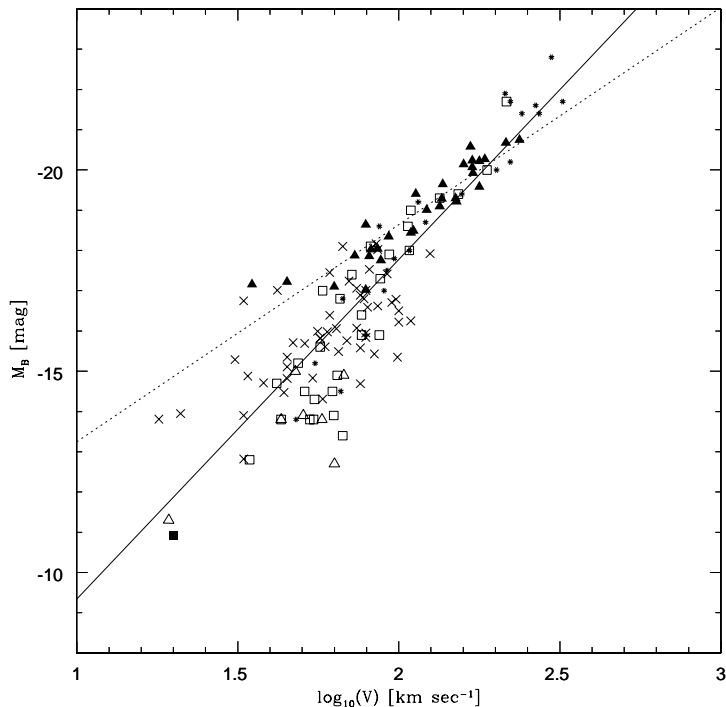


Fig. 9. Absolute B magnitude vs the log of the maximum rotation velocity. Stars are galaxies from Broeils (1992), empty triangles galaxies from Côté et al. (2000), filled triangles from Verheijen (1997), empty squares from Stil (1999) and crosses from Swaters (1999). Cam B is shown by a filled hexagon (where the “asymmetric drift” corrected velocity is used) and an empty hexagon (where the observed peak velocity is used). The dotted line is the best fit to the galaxies from the Verheijen (1997) sample alone, while the solid line is the best fit to the entire sample.

6 Discussion

The mass of the gas disk in Cam B is $M_{gas}=6.6 \times 10^6 M_{\odot}$ and the adopted ($\Upsilon_V = 1$) model gives the mass of stellar disk to be $M_*=3.5 \times 10^6 M_{\odot}$. From the last measured point of the observed rotation curve, we get a total dynamical mass of $M_T=1.1 \times 10^8 M_{\odot}$, i.e. at the last measured point more than 90% of the mass of Cam B is dark. Like other faint dwarf galaxies, Cam B is also dark matter dominated in the inner regions, by the time one reaches a galactocentric radius of two (optical) disk scale lengths, the mass of the stellar and gas disks is small compared to the mass in the dark matter.

In Fig. 9 the maximum rotation velocity for Cam B (after correction for “asymmetric drift”) is plotted against the absolute blue magnitude. The same quantities for several other spiral and dwarf galaxies with measured HI rotation curves are also shown. The samples from which these galaxies have been drawn are listed in the figure caption. A clear trend is seen between the maximum

velocity and absolute magnitude (which is of course the basis of Tully-Fisher relationship). We are forced to use the blue magnitude (even though it is in general a poor quantity for this purpose, see below) because it is the only band for which measurements exist for both Cam B as well as all the other samples that we have used. Primarily because of uncertain and absolute magnitude dependent internal extinction corrections, the B band Tully-Fisher relationship has been the subject of recent debate. Stil (1999) noted that dwarf galaxies lie systematically below the Tully-Fisher relationship defined by bright galaxies (the dotted line in Fig. 9) i.e. dwarfs are comparatively underluminous for their given circular velocity. Swaters (1999) noted the same effect for the R band Tully-Fisher relationship and suggested that the problem could be ameliorated by applying a “baryonic correction” i.e. a correction for the fact that dwarf galaxies have still to convert much of their gas into stars. Pierini (1999) found that the adopted correction for internal extinction makes a substantial difference to the slope of the B band Tully-Fisher relationship, and that depending on the internal extinction correction applied one could reduce (but not completely eliminate) the need for a baryonic correction. Finally, Mcgaugh et al. (2000) state that due to the problem of internal extinction the blue band Tully-Fisher relation actually gives no clear evidence for the need for a baryonic correction, but that the need for such a correction is clear when one uses near infrared absolute magnitudes (i.e. bands which are little affected by internal extinction).

The galaxy magnitudes in Fig. 9 range from $M_B \sim -23$ to $M_B \sim -11$, and we also show in the figure the best fit straight line (the solid line) between M_B and V_{max} over this entire magnitude range. Cam B lies close to this line if one uses the “asymmetric drift” corrected rotation velocity. The scatter about the best fit line is ~ 1 magnitude, a large part of this is probably due to (i) uncertainties in the distances to the galaxies, and (ii) the different prescriptions for correcting for internal extinction that have been applied to the different samples. As expected from the discussion above, one can see that galaxies with large velocity widths lie systematically above this best fit slope, while galaxies with low velocity widths lie systematically below this slope (with the break occurring at $\sim 100 \text{ km sec}^{-1}$ – this corresponds well to the break velocity seen in the near infrared Tully-Fisher diagram, (Mcgaugh et al. 2000)).

Finally we note that Fig. 9 does not show any particular flattening of the slope around $M_B = -14.0$ (as claimed by Côté, Carignan & Freeman (2000)). Part of the reason for this difference is probably that Côté, Carignan & Freeman (2000) used rotation velocities from the Lo, Sargent & Young (1993) sample, while we have not. The observations of (Lo, Sargent & Young 1993) used a velocity resolution of $\sim 6.5 \text{ km sec}^{-1}$, and also often lacked sensitivity to the low extended HI distribution, for both of these reasons the V_{max} of the galaxies in this sample could be underestimated (see eg. Skillman 1996, Hoffman 1996).

In Sec. 1 we had discussed that based on galaxy formation simulations, several authors have suggested that smaller galaxies should in general have a higher central halo density than bigger galaxies. We plot in Fig. 10 the halo density of galaxies (drawn from the same samples as for Fig. 9, except that the sample from (Stil 1999) had to be dropped since mass decompositions were not available for this sample) as a function of their circular velocity (panels [A] & [B]) and as a function of the absolute blue magnitude (panels [C] & [D]). From the raw data itself one finds in general no clear correlation between halo density and blue magnitude or circular velocity. To see if this the effect of a large scatter, we also bin the data in 4 bins and show the median halo density in each bin (the solid points). As can be seen the binned data do show a trend of increasing halo density with decreasing blue luminosity or circular velocity. Interestingly, the correlation is sharper when the Ursa Major sample of (Verheijen 1997) is excluded (panels [B] & [D]). If this is a real effect, then it is perhaps related to the higher mean galaxy density of the Ursa Major sample. The solid lines shown in panels [B] & [D] are $\rho_0 \propto V_{max}^{-0.85}$ and $\rho_0 \propto M_B^{0.25}$ respectively. We also note that the halo densities being plotted have been computed for “maximum disk” modified isothermal halo fits, and that the correlation we find is related to (but not identical to) the statement often made in the literature that the in centers of large galaxies the baryonic mass is more dominant than in the centers of dwarf galaxies.

To conclude, we have presented optical images and HI 21cm synthesis data for the faint dwarf galaxy Cam B. We find that Cam B has a very regular velocity field that can be well fit with the standard tilted ring model, despite the fact that its observed peak rotation velocity is of the same order of magnitude as the random motions of the gas. The very high velocity resolution of our observations ($\sim 1.6 \text{ km sec}^{-1}$) were crucial in order to determine the systematic patterns in the velocity field of the HI disk. Mass modeling of the galaxy shows that its rotation curve can be well fit by a constant density halo, with density $\sim 12 \times 10^{-3} M_\odot \text{pc}^{-3}$. This measurement of the halo central density is not very sensitive to the assumed mass to light ratio (Υ_V) of the stellar disk. Like other faint dwarf galaxies the mass of Cam B is dominated by the dark matter halo; at the last measured point $> 90\%$ of the mass is in the dark halo. The dominance of the dark matter halo together with the linear shape of the rotation curve (after correction for “asymmetric drift”) mean that one cannot obtain a good fit to the rotation curve using a NFW halo regardless of the assumed Υ_V . Finally, combining the data for Cam B with the data available in the published literature for other dwarf and normal disk galaxies, we find a weak trend for the central halo density to decrease with increasing galaxy size.

Acknowledgements: These observations would not have been possible without the many years of dedicated effort put in by the GMRT staff in order to build the telescope. The GMRT is operated by the National Centre for Radio

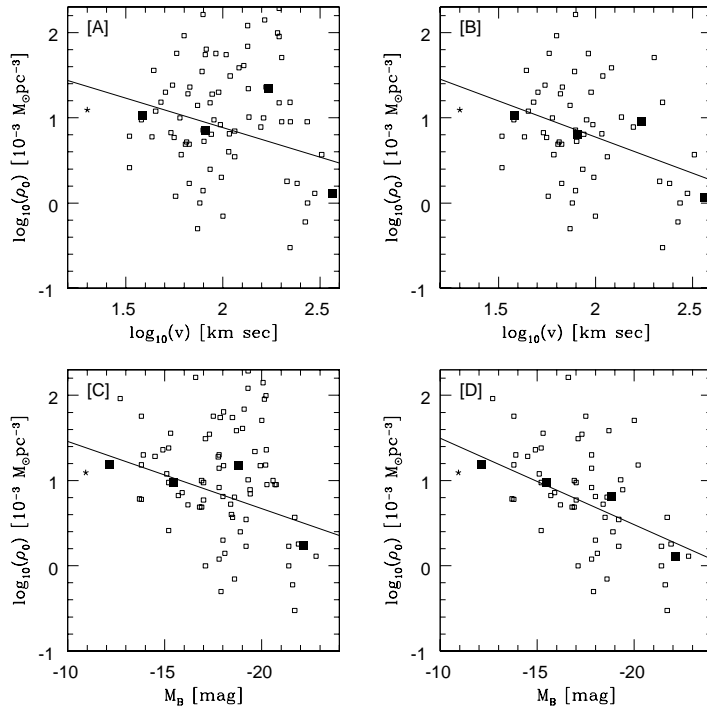


Fig. 10. Scatter plots of the central halo density against the circular velocity (panels [A] and [B]) and the absolute blue magnitude (panels [C] and [D]). The data (empty squares) are from Verheijen (1997), Broeils (1992), Côté et al. (2000) and Swaters (1999). The filled squares are the medians of the binned data, and the straight lines are the best fits to the binned data. Cam B is shown as a star.

Astrophysics of the Tata Institute of Fundamental Research. We are grateful to D. J. Bomans for generously sharing his data and results prior to publication.

References

- Bell E. F., & de Jong, R. S., Stellar mass-to-light ratios and the Tully-Fisher relation, 2001, *ApJ* 550, 212-229. (2001ApJ...550..212B)
- Bender, R., & Möllenhoff, C., Morphological analysis of massive early-type galaxies in the Virgo cluster, 1987, *A&A* 177, 71-83. (1987A&A...177...71B)
- van den Bosch, F. C. & Swaters, R. A., Dwarf galaxy rotation curves and the core problem of dark matter haloes, 2001, *MNRAS* 325, 1017-1038. (2001MNRAS.325.1017V)
- Bottema, R, Shostak, G. S., & van der Kruit, P. C., The thickness of the hydrogen layer of the edge-on dwarf galaxy NGC 5023, 1986, *A&A* 167, 34-40. (1986A&A...167...34B)

- Broeils, A. 1992, Ph.D. thesis. Rijksuniversiteit Groningen.
- Carignan, C., & Freeman, K. C., DDO 154 - A 'dark' galaxy?, 1988, *ApJL* 332, 33-36. (1988ApJ...332L..33C)
- Carignan, C., Beaulieu, S. & Freeman, K. C. At The Low-Mass End: Light and HI distribution of GR 8, 1990, *AJ* 99, 178-190. (1990AJ.....99..178C)
- Casertano S., Rotation curve of the edge-on spiral galaxy NGC 5907: disc and halo masses, 1983, *MNRAS* 203, 735-747. (1983MNRAS.203..735C)
- Christian, C. A., Adams M., Barnes J.V., Butcher H., Mould J.R., & Siegel M., 1985, *PASP* 97, 363-372. (1985PASP...97..363C)
- Côté S., Carignan, C. & Freeman, K. C., The Various Kinematics of Dwarf Irregular Galaxies in Nearby Groups and Their Dark Matter Distributions, 2000, *AJ* 120, 3027-3059. (2000AJ....120.3027C)
- de Grijs, R. & Peletier, R. F., The shape of galaxy disks: how the scale height increases with galactocentric distance, 1997, *A&A* 320, L21-24. (1997A&A...320L..21D)
- Hoffman, G. Lyle, Salpeter, E. E., Farhat, B., Roos, T., Williams, H., & Helou, G., Arecibo HI mapping of a large sample of dwarf irregular galaxies, 1996, *ApJS* 105, 269-298. (1996ApJS..105..269H)
- Huchtmeier, W. K., Karachentsev, I. D., Karachentseva, V. E., & Ehle, M., HI observations of nearby galaxies I. The first list of the Karachentsev catalog, 2000, *A&AS* 141, 469-490. (2000A&AS..141..469H)
- Israel, F. P., Tacconi, L. J. & Bass, F., CO observations of 25 dwarf galaxies, 1995, *A&A* 295, 599-604. (1995A&A...295..599I)
- Klypin, A. A., Kravtsov, A. V., Bullock, J. S. & Primack, J. R., Resolving the Structure of Cold Dark Matter Halos, 2001, *ApJ* 554, 903-915. (2001ApJ...554..903K)
- Lake, George, Schommer, R. A. & Van Gorkom, J. H., The distribution of dark matter in the dwarf galaxy DD0 170, 1990, *AJ* 99, 547-560. (1990AJ...99...547L)
- Landolt A. U., UBVRI photometric standard stars around the celestial equator, 1983, *AJ* 88, 439-460. (1983AJ.....88..439L)
- Lo, K.Y., Sargent, W. L. W., & Young, K., The H I structure of nine intrinsically faint dwarf galaxies, 1993, *AJ* 106, 507-529. (1993AJ....106..507L)
- McGaugh, S. S., Schombert, J. M., Bothun, G. D., & de Blok, W. J. G., The Baryonic Tully-Fisher Relation, 2000, *ApJL* 533, 99-102. (2000ApJ...533L..99M)
- Meurer, G. R., Carignan, C., Beaulieu, S. F., & Freeman, C. F., NGC 2915. II. A dark spiral galaxy with a blue compact dwarf core, 1996, *ApJ* 111, 1551-1771. (1996AJ....111.1551M)

- Navarro, J. F., Frenk, C. S. & White S. D. M., The Structure of Cold Dark Matter Halos, 1996, ApJ 462, 563-575. (1996ApJ...462..563N)
- Navarro, J. F., Frenk, C. S. & White S. D. M., A Universal Density Profile from Hierarchical Clustering, 1997, ApJ 490, 493-508. (1997ApJ...490..493N)
- Navarro, J. F., Dark Matter Halos and Disk Rotation Curves, 1998, ASP Conf. Series, 136, 409-417. (1998gaha.conf..409N)
- Pierini, D., Internal extinction, population incompleteness bias and the faint-end of the B-band Tully-Fisher relation, 1999, A&A 352, 49-63. (1999A&A..352...49P)
- Schlegel, D. J., Finkbeiner, D. P., & Davis, M., Maps of Dust Infrared Emission for Use in Estimation of Reddening and Cosmic Microwave Background Radiation Foregrounds 1998, ApJ 500, 525-553. (1998ApJ...500..525S)
- Skillman, E. D., Neutral Hydrogen in Dwarf Galaxies, 1996, PASP Conf. Ser., 106, 208-230. (BIBCODE-XXX)
- Skillman, E. D., Terlevich, R., Teuben, P. J. & Van Woerden, H., HI synthesis observations of the dwarf irregular galaxy Sextans A, 1988, A&A 198, 33-42. (1988A&A..198...33S)
- Stil J.N., 1999, Ph.D. thesis, Rijksuniversiteit Leiden.
- Swarup G., Ananthkrishnan S., Kapahi V. K., Rao A. P., Subrahmanya C. R., & Kulkarni V. K., The Giant Meterwave Radio Telescope, 1991, Current Science, 60, 95.
- Swaters, R., 1999, Ph.D. thesis, Rijksuniversiteit Groningen.
- van der Kruit, P.C., Searle, L., Surface photometry of edge-on spiral galaxies. I - A model for the three-dimensional distribution of light in galactic disks. II - The distribution of light and colour in the disk and spheroid of NGC 8911981, A&A 95, 105-126. (1981A&A....95..105V)
- Taylor, C. L., Kobulnicky, H. A. & Skillman, E. D., CO Emission in Low-Luminosity, H I-rich Galaxies, 1998, AJ 116, 2746-2756. (1998AJ....116.2746T)
- Verheijen, M.A.W, 1997, PhD thesis, Rijkuniversiteit Groningen.